PAPER • OPEN ACCESS

Effects of heavy Si doping on the structural and optical properties of n-GaN/AlN/Si(111) heterostructures

View the article online for updates and enhancements.

Materials Research Express

PAPER

Effects of heavy Si doping on the structural and optical properties of n-GaN/AlN/Si(111) heterostructures

M A Zambrano-Serrano[1], **Carlos A Hernández**[2], **O de Melo**[3], **M Behar**[4], **S Gallardo-Hernández**[1] ,
Y L Casallas-Moreno[5], **A Ponce**[6] , **A Hernandez-Robles**[6], **D Bahena-Uribe**[7], **C M Yee-Rendón**[8] and
M López-López[1]

1   Centro de Investigación y Estudios Avanzados del IPN, Apartado Postal 14-740, Ciudad de Mexico, 07360, Mexico
2   Tecnológico Nacional de México/Instituto Tecnológico de Tuxtla Gutiérrez, Carretera Panamericana km 1080, C.P. 29050, Tuxtla Gutiérrez, Mexico
3   Facultad de Física, Universidad de la Habana, Colina Universitaria 10400. La Habana, Cuba
4   Ion Implantation Laboratory, Physics Institute, Federal University of Rio Grande do Sul, CP 15051, CEP 91501-970, Porto Alegre, RS, Brazil
5   CONACYT-Unidad Profesional Interdisciplinaria en Ingeniería y Tecnologías Avanzadas,Instituto Politécnico Nacional, Av. IPN 2580, Gustavo A. Madero, 07340 Ciudad de México, Mexico
6   Department of Physics and Astronomy, University of Texas at San Antonio, San Antonio, Texas 78249, United States of America
7   Advanced Laboratory of Electron Nanoscopy, CINVESTAV, Av. IPN 2508, 07360 Mexico City, Mexico
8   Facultad de Ciencias Fisico-Matematicas, Universidad Autonoma de Sinaloa, Cd. Universitaria, Culican SIN, 80000, Mexico

E-mail: mlopezl@cinvestav.mx

Abstract

n-GaN/ AlN heterostructures were grown by molecular beam epitaxy on Si(111) substrates.The GaN films were n-type doped with silicon and the effect of doping concentration on the structural and optical properties was studied. Si doping promotes a reduction of dislocation density as revealed by x-ray data analysis and Transmission Electron Microscopy. Furthermore, a decrease in the yellow band measured by Photoluminescence Spectroscopy was observed when silicon doping concentration was increased up to 1.7×10^{19} atoms cm^{-3}. A particular mosaic structure was induced by the Si-doping as inferred from Rutherford Backscattering measurements. The crystal quality shows a small degradation for very heavily doped samples (1.3×10^{20} atoms cm^{-3}).

1. Introduction

The growth of III-N semiconductors has made great progress in recent years, however, studies are still required in areas such as heteroepitaxy [1], doping [2] and nanostructuring [3, 4]. In particular, the heteroepitaxy of GaN on Si is the fundamental basis for a variety of important electronic devices [1]. The large mismatch in lattice constants and thermal expansion coefficients between GaN and Si result in a very high density of crystal defects that strongly degrade devices performance. For this reason, the study of growth mechanisms and processes that improve the GaN epitaxial quality is a subject of current interest [5]. Early in the 90′s, Watanabe *et al* proposed the use of an AlN intermediate layer to avoid the formation of amorphous SiN at the GaN/Si interface due to the strong chemical reactivity between Si and N [6]. On the other hand, silicon is the preferred element for GaN n-type doping, the effects of Si on optical and structural properties have been widely studied [7–11]. It was reported that at low doping levels Si tends to deteriorate the optical and structural properties of GaN [9, 10]. However, this result has been the subject of controversy [10, 11], which becomes more important at high Si concentrations [12]. Sanchez *et al* reported the effect of high silicon doping exhibiting an improvement in crystal quality by reducing the dislocation density as Si doping increases from 10^{17} to 6×10^{18} cm^{-3} [13]. In this work we have studied the optical and structural properties of n-GaN/AlN/Si heterostructures, aiming to contribute to the understanding of the effects of Si doping of GaN, in particular in the heavily doped regime (10^{18}–10^{20} Si-atoms cm^{-3}).

Table 1. Silicon concentrations, lattice constant values, and dislocation densities obtained in the samples.

Sample	Si concentration atoms cm^{-3}	c constant (Å)	a constant (Å)	FWHM omega (degrees)	Screw dislocation density (cm^{-2})
S1	3.2×10^{18}	5.1847	3.1892	0.8	1.66×10^{10}
S2	6.1×10^{18}	5.1869	3.1886	0.44	5.08×10^{9}
S3	1.7×10^{19}	5.1866	3.1887	0.37	3.57×10^{9}
S4	1.3×10^{20}	5.1851	3.1891	0.46	5.57×10^{9}

2. Experimental

The heterostructures were grown in a Riber C21 molecular beam epitaxy (MBE) system. Si(111) substrates were chemically cleaned employing the Ishizaka and Shiraki method [14]. In order to desorb surface oxides, the substrates were annealed at 900 °C. After this, the substrate temperature was decreased to 750 °C, at this temperature, the 7 × 7 surface reconstruction was monitored by Reflection High-Energy Electron Diffraction (RHEED). In order to avoid the degradation of the Si substrate by the exposition to nitrogen [6], a metallization of the Si surface was performed with an aluminum layer (~5 monolayers) deposited at 850 °C. After this process, an AlN layer was grown at 850 °C with a nominal thickness of 30 nm. Active N flux was provided by RF-plasma source operated at 150W with N$_2$ flow of 0.25 sccm. The ratio of III/N fluxes was higher than one to ensure a metallic rich growth condition that leads to a smoother surface [15]. GaN layers with thickness of 1.4 μm were grown and doped with different silicon concentrations by varying the temperature of the silicon effusion cell.

    The Si doping levels in the samples were examined by Secondary Ion Mass Spectroscopy (SIMS) employing a magnetic sector spectrometer Cameca ims-6f to analyze the silicon distribution through the samples. We obtained Si concentrations in the range of 3.2×10^{18} to 1.3×10^{20} atoms cm^{-3}, as presented in table 1. The GaN structural analysis was performed by High Resolution x-ray Diffraction (HRXRD) $\omega-2\theta$ scans and rocking curves using a Panalytical X'pert Pro diffractometer. Samples for cross-sectional- and plan-view transmission electron microscopy (TEM) studies, were prepared by focused ion beam (FIB). Raman Spectroscopy technique was employed with a Thermo Scientific Raman Microscope model DXR. Backscattering configuration was used with a 20x objective and 532 nm wavelength with 1 mW power. Rutherford back scattering (RBS) measurements were performed in the Tandetron accelerator of the Physics Institute of the Universidade Federal do Rio Grande do Sul using the beamline of 3.035 MeV (α-particles). The composition, stoichiometry and thickness of the samples were determined from the RBS spectra analysis by using the SIMNRA code [16]. In all cases the reduced quadratic deviation, χ^2 per channel, between experimental data and simulation was kept below 5 as it is considered an indication of acceptable simulation for RBS. Surface roughness was taking into consideration as usually, simulating the tails of the corresponding plateaus in the RBS spectra.
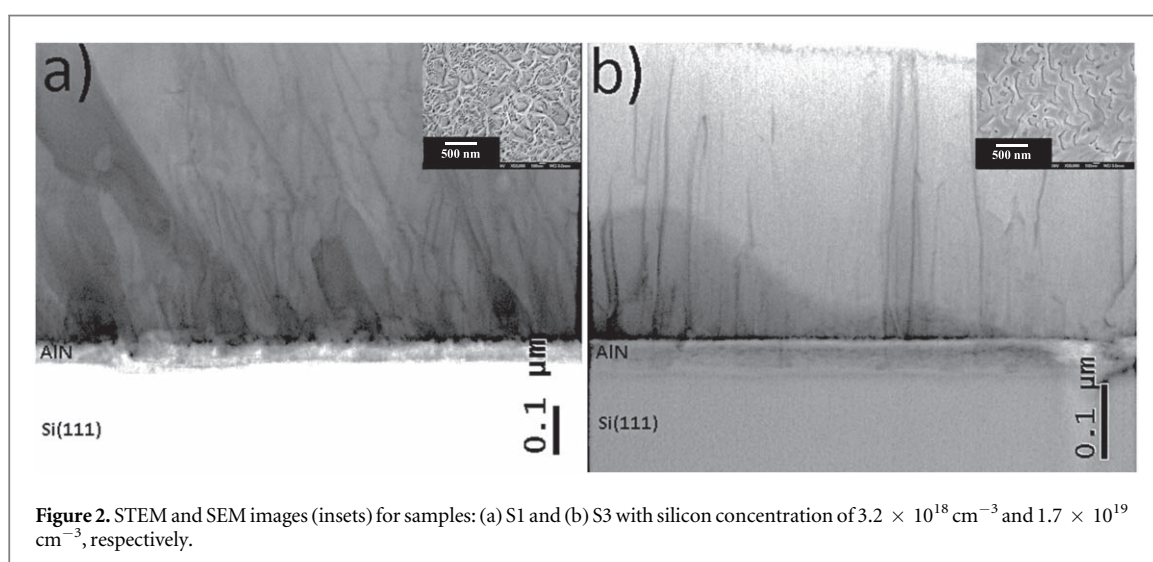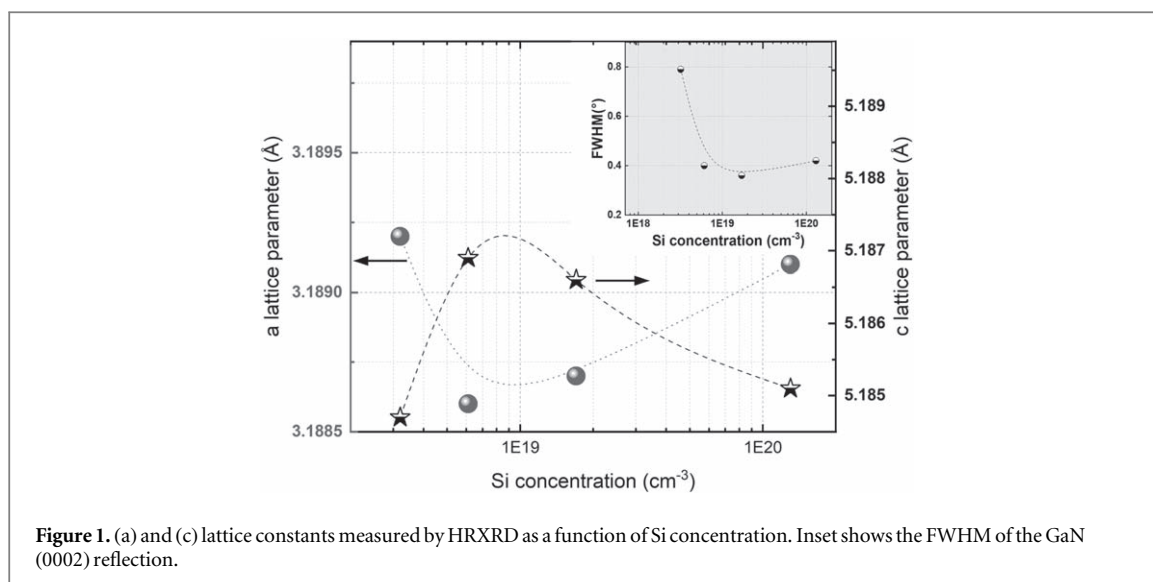
3. Results and discussion

Figure 1 shows the variation of the GaN lattice parameters (a and c) calculated from HRXRD as a function of Si doping concentration. The c parameter was obtained directly from the (0002) plane reflection, while the a lattice constant was obtained through the asymmetric (1011) plane [17]. From the obtained a and c values (table 1), we observe that the samples suffer from residual strain. The c/a ratio approached the ideal value (1.63 in a hcp structure) for samples S2 and S3 (c/a = 1.626) with a Si concentration of 6.1×10^{18} and 1.7×10^{19} atoms cm^{-3}, respectively, as we will show sample S3 presented the best optical and structural properties. The densities of screw dislocations were calculated using the method described in ref. [18]. The minimum of dislocation density was obtained for S3, as can be seen in table 1.

    The inset in figure 1 shows the full width at half maximum (FWHM) for rocking curves of the GaN(0002) reflection. These measurements showed a positive effect on the crystalline quality of the GaN layer as the silicon concentration was increased. The sample S1 with the lower silicon concentration exhibited the worst crystalline quality, the FWHM dropped for higher Si concentrations up to 1.7×10^{19} cm^{-3}. The crystal quality was slightly degraded for the sample S4 with a Si doping of 1.3×10^{20} cm^{-3}, as evidenced by a small increase of the FWHM of the rocking curves.

    Sánchez *et al* [19] from a High Resolution Electron Microscopy study concluded that the Si doping produces a decrease of the threading dislocation density but also leads to an increase of planar defect density. The Si doping affects both the grain size and misorientation in GaN. The increase in the tilt of GaN grains and in the planar defect density could be the cause of the reduction in dislocation density in GaN doped with Si [19].

    We analyzed our samples by scanning transmission electron microscopy (STEM) to observe the effects of silicon doping on crystal structure. In figure 2 we present cross-section STEM images corresponding to samples

Figure 1. (a) and (c) lattice constants measured by HRXRD as a function of Si concentration. Inset shows the FWHM of the GaN (0002) reflection.

Figure 2. STEM and SEM images (insets) for samples: (a) S1 and (b) S3 with silicon concentration of 3.2×10^{18} cm^{-3} and 1.7×10^{19} cm^{-3}, respectively.

S1 and S3, the insets show the corresponding surface images by scanning electron microscopy (SEM). In order to clarify the crystallographic orientation relationship between GaN and Si substrate, selected area electron diffraction (SAED) patterns were collected at different positions of samples. Figure 3 shows SAED patterns registered at (a) the GaN film, (b) the interface between substrate and epilayer, where the epitaxial relationship is presented, and (c) the substrate, as a reference. From the cross-sectional STEM images of figure 2 we confirm a large reduction of the density of dislocations for sample S3. Moreover, the formation of a mosaic structure is clearly observed in the SEM image of the inset in figure 2(b). As we will show below, the particular orientation of the columnar grains that compose this mosaic structure has a strong impact on the behavior of RBS spectra.

In wurtzite-type GaN films there are three types of Burgers vectors of perfect dislocations: i) $a = 1/3\langle 11\bar{2}0\rangle$, ii) $c = \langle 0001\rangle$ and iii) $a + c = 1/3\langle 11\bar{2}3\rangle$. The dislocations associated with these Burgers vectors are: (i) edge dislocations (type A), (ii) screw dislocations (type B), and (iii) mixed dislocations (type C). The propagation of edge dislocations takes place on planes of the type $\{1\bar{1}00\}$. These dislocations can have six $a = 1/3\langle 11\bar{2}0\rangle$ equivalent Burgers vectors. In order to image the edge type dislocations, weak beam (WB) planar view TEM (PVTEM) images were collected along the [0001] zone axis and the two beam conditions.

The SAED pattern collected along the [0001] zone axis is presented in figures 4(a), and (b) is the PVTEM image showing edge type dislocations for sample S1. The edge dislocations measured from the PVTEM image, figure 4(c), gives 1.2×10^{11} dislocations cm^{-2}. That is, the number density of edge type dislocations is one order of magnitude larger compared to that of screw type dislocations obtained by HRXRD.

Figure 5 shows the RBS spectra corresponding to (a) a non-intentionally doped GaN/AlN/Si(111) sample and (b) the sample S3, obtained with 3.035 MeV α-particles incident beam. In these conditions, nitrogen signal is practically no detectable due to the low atomic mass of N (spectra acquired for both samples with a proton
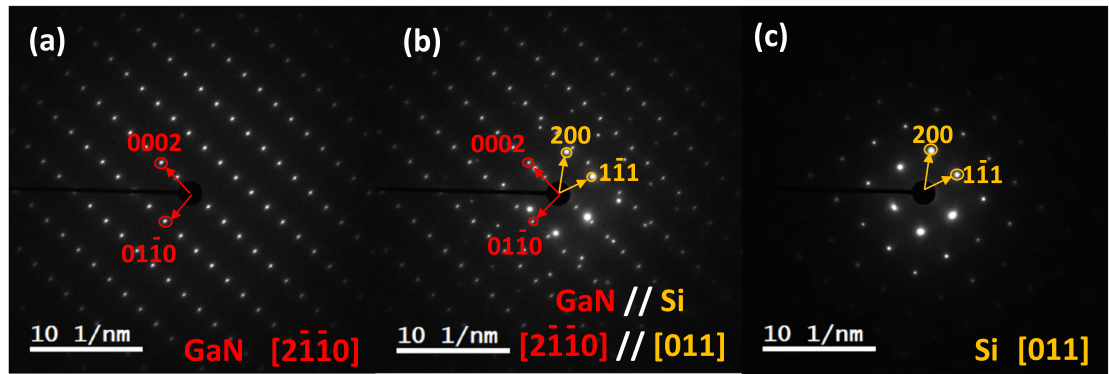
Figure 3. SAED patterns collected at: (a) GaN film, (b) the Si-epilayer interface, and (c) the substrate.
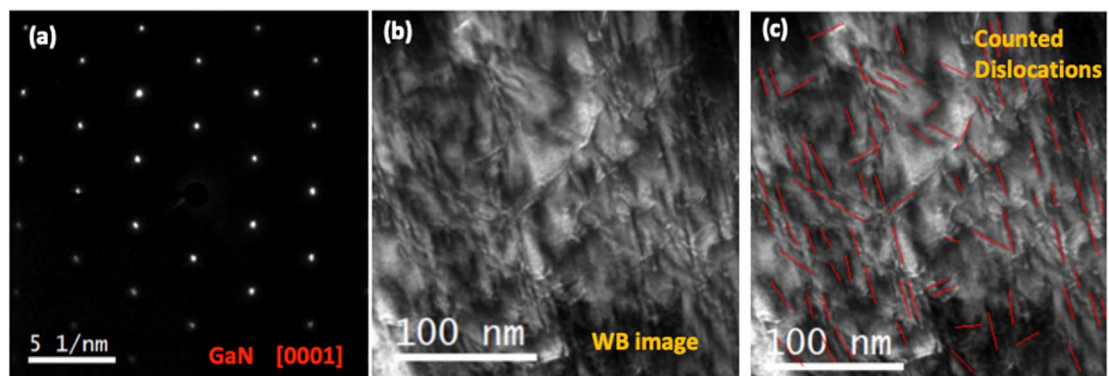

Figure 4. (a) SAED pattern collected along the [0001] zone axis and the two beam conditions to image the edge dislocations in sample S1, (b) PVTEM image employed to count (c) the edge type dislocations.

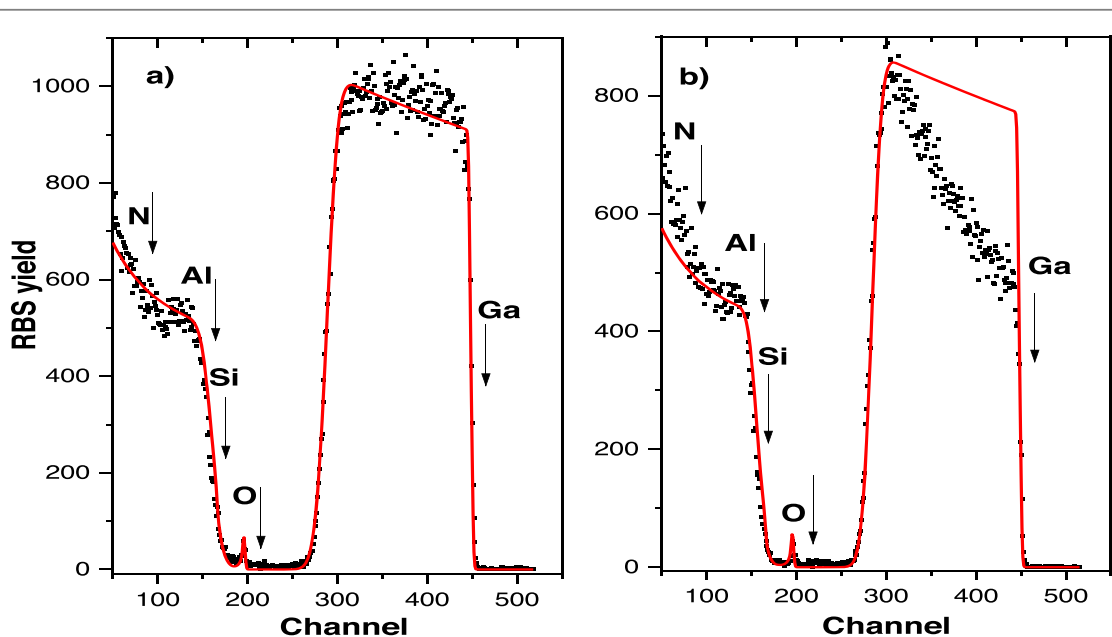**Figure 5.** (a) RBS spectrum of a non-intentionally doped GaN sample and (b) sample S3 with a doping silicon concentration of 1.7×10^{19} cm^{-2}. The simulation using SIMNRA code are the red-colored curves in the spectra. Surface signals for Ga, O, Al, Si and N are represented by arrows (channel, **ch**, can be converted to energy, **E**, by using the linear relation $E = 90\ keV + 5.2\ \frac{keV}{ch} * ch$).
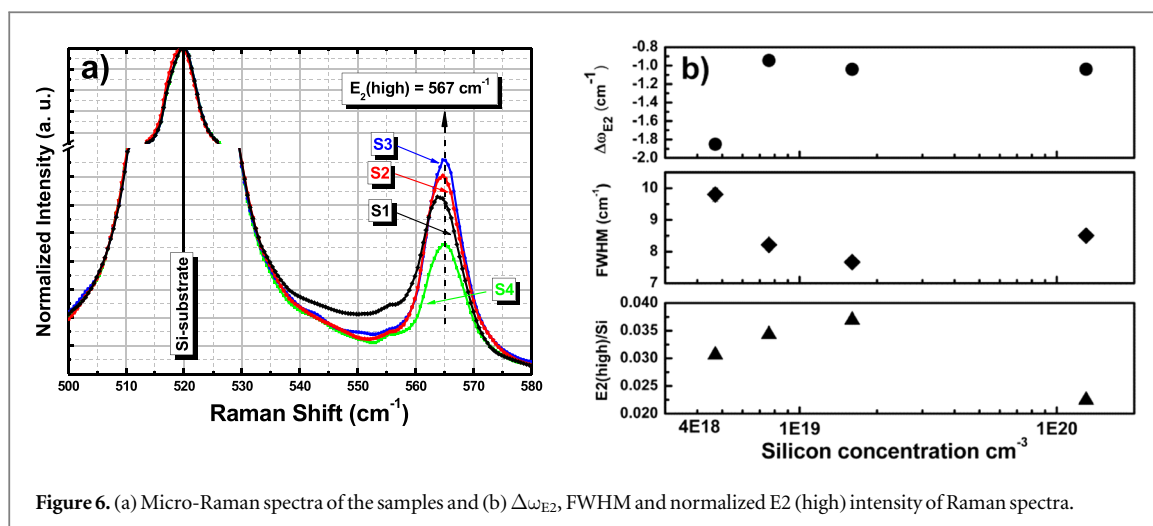
Figure 6. (a) Micro-Raman spectra of the samples and (b) $\Delta\omega_{E2}$, FWHM and normalized E2 (high) intensity of Raman spectra.

beam, in which the N signal is enhanced, are presented at the supplementary information). For the spectra simulation, we consider that all the N atoms are forming GaN; then, a stoichiometric amount of that element with respect to Ga was considered. In principle, for the Si-doped sample the amount of the Si dopant is too small to expect an appreciable contribution to the RBS spectrum. The surface signal positions for Ga, O and Si (coming from the Si substrate and considerably shifted to lower energies due to the large thickness of the GaN film) are indicated by arrows. The Al signal coming from the buffer layer, also shifted to lower energies, it is overlapped with the much larger silicon signal. The small oxygen signal corresponds to the expected surface oxidation in samples exposed to air and was fitted as Ga oxide.

We observe that the fitting reproduces very well the spectrum in figure 5(a), however for the Si-doped sample there is a strong decrease in the Ga signal with increasing energy, which was not possible to fit considering an arbitrarily oriented crystal. This is the expected behavior for spectra acquired at partial channeling conditions [20]. However, is important to note that the sample was not intentionally positioned at channeling conditions. The channeling-like spectra can be explained considering that the columnar grains have a random distribution of small tilt angles, such that at a given arbitrary RBS measurement there is a considerable number of columnar grains aligned at channeling condition producing the characteristic spectra in figure 5(b).

Additional structural characterization was carried out using micro-Raman technique, which was performed at room temperature (RT). In figure 6, we show the Raman spectra of the samples.

The strongest signal is associated with the silicon substrate, which is located at 520 cm^{-1}. All spectra have been normalized to the substrate signal. At 567 cm^{-1} (dotted vertical line), we found the E2 (high) mode signal of GaN [21]. In figure 6(b), we present the shift $\Delta\omega_{E2}$, the FWHM and the normalized intensity of the E2(high) peak as a function of silicon concentration. We observe that the FWHM of the E2 mode decreases and its intensity increases with the amount of Si, presenting a minimum FWHM- and a maximum intensity for sample S3. As for $\Delta\omega_{E2}$, all the samples presented red-shifts in the E2(high) peak position, which are associated with lattice tensile stress [22]. The sample S1 (with Si-doping in the order of 10^{18} atoms cm^{-3}) has the largest red-shift of -1.85 cm^{-1}, corresponding to a tensile stress of 0.63 GPa, as calculated by the method described by Kisielowski *et al* [23]. For the samples with the highest Si-doping (S3 and S4) the tensile stress decreases to 0.35 GPa. The tensile stress is expected to affect GaN optical properties.

Photoluminescence spectroscopy (PL) for the samples was performed at room temperature employing a HeCd laser (325 nm). The PL spectra are shown in figure 7, we observe a yellow band emission (see inset in the figure) for the doped samples in the order of 10^{18} atoms cm^{-3} (S1, S2), this band disappears for samples (S3, S4) with doping higher than 10^{19} atoms cm^{-3}. We relate the yellow emission mitigation with the reduction of dislocation density [24]. Besides, for all the samples the most intense PL peak is red-shifted compared to the 300K-GaN band gap energy of 3.4 eV. Impurity related emissions, like donors to acceptors transitions could contribute to the PL red-shift [25]. However, is important to note that at heavy doping concentration, in addition to stress, other phenomena such as: band gap renormalization (BGR) and Burstein-Moss shift (BMS), affect the band gap energy value [12, 26].

4. Conclusions

We performed a study of the structural and optical properties of n-GaN/AlN/Si(111) heterostructures with a high n-GaN doping in the range of 3.2×10^{18} to 1.3×10^{20} Si-atoms cm^{-3}. As the results, GaN crystal quality

Figure 7. PL spectra at room temperature as a function of silicon concentration.
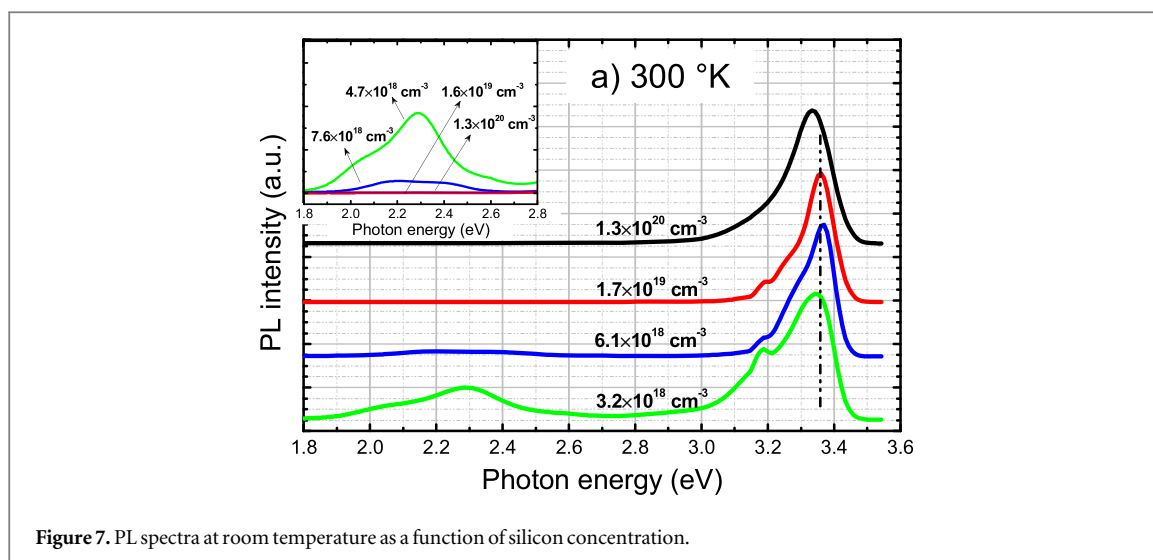
increased with the silicon doping, the best crystal quality was obtained for a Si concentration of 1.7×10^{19} atoms cm^{-3}. The Si-doped samples presented a channeling-like RBS spectrum which was explained by the mosaic structure produced by columnar grains with a random distribution of tilt angles. Increasing the doping concentration up to 1.3×10^{20} atoms cm^{-3} produces a small degradation of the GaN structural- and optical properties as evaluated by XRD, TEM, Raman spectroscopy and PL.

Acknowledgments

Data availability statement

The data that support the findings of this study are available upon reasonable request from the authors.

ORCID iDs

S Gallardo-Hernández ⦿ https://orcid.org/0000-0001-6968-5560
A Ponce ⦿ https://orcid.org/0000-0001-5529-6468
C M Yee-Rendón ⦿ https://orcid.org/0000-0003-2397-9066
M López-López ⦿ https://orcid.org/0000-0002-4647-6683

References

[1] Zhang Y, Dadgar A and Palacio T 2018 Gallium nitride vertical power devices on foreign substrates: a review and outlook *J. Phys. D: Appl. Phys.* **51** 273001 and references therein
[2] Liang Y-H and Towe E 2018 Progress in efficient doping of high aluminum-containing group III-nitrides *Appl. Phys. Rev.* **5** 011107
[3] Li E, Wu G, Cui Z, Ma D, Shi W and Wang X 2016 Enhancing the field emission properties of Se-doped GaN nanowires *Nanotechnology* **27** 265707
[4] Cuia Z, Lia E, Kea X, Zhaoa T, Yanga Y, Dingb Y, Liuc T, Qua Y and Xua S 2017 Adsorption of alkali-metal atoms on GaN nanowires photocathode *Appl. Surf. Sci.* **423** 829–35
[5] Tanaka A, Choi W, Chen R, Liu R, Mook W M, Jungjohann K L, Yu P K L and Dayeh S A 2019 Structural and electrical characterization of thick GaN layers on Si, GaN, and engineered substrates *J. Appl. Phys.* **125** 082517
[6] Watanabe A, Takeuchi T, Hirosawa K, Amano H, Hiramatsu K and Akasaki I 1993 The growth of single crystalline GaN on a Si substrate using AlN as an intermediate layer *J. Cryst. Growth* **128** 391–6
[7] Fritze S, Dadgar A, Witte H, Bügler M and Rohrbeck A 2012 High Si and Ge n-type doping of GaN doping-Limits and impact on stress *Appl. Phys. Lett.* **100** 122104
[8] Reshchikov M A and Morkoç H 2005 Luminescence properties of defects in GaN *J. Appl. Phys.* **97** 061301
[9] Zhao D G, Jiang D S, Zhu J J, Liu Z S and Zhang S M 2007 Does an enhanced yellow luminescence imply a reduction of electron mobility in n-type GaN ? *J. Appl. Phys.* **102** 113521

[10] Lee I H, Choi I H, Lee C R, Son S J, Leem J Y and Noh S K 1997 Mobility enhancement and yellow luminescence in Si-doped GaN grown by metalorganic chemical vapor deposition technique *J. Cryst. Growth* **182** 314

[11] Moram M A, Kappers M J, Massabuau F, Oliver R A and Humphreys C J 2011 The effects of Si doping on dislocation movement and tensile stress in GaN films *J. Appl. Phys.* **109** 073509

[12] Lingaparthi R, Dharmarasu N and Radhakrishnan K 2022 Effects of Si doping well beyond the Mott transition limit in GaN epilayers grown by plasma-assisted molecular beam epitaxy *J. Phys. D: Appl. Phys.* **55** 095110

[13] Sánchez-Garcia M A, Calleja E, Naranjo F B, Sánchez F J, Calle F, Muñoz E, Sánchez A M, Pacheco F J and Molina S I 1999 MBE growth of GaN and AlGaN layers on Si (111) substrates: doping effects *J. Cryst. Growth* **415** 201

[14] Ishizaka A and Sharaki Y 1986 Low temperature surface cleaning of silicon and its application to silicon MBE *J. Electrochem. Soc.* **133** 666

[15] Adelmann C, Brault J, Jalabert D, Gentile P, Mariette H, Mula G and Daudin B 2002 Dynamically stable gallium surface coverages during plasma-assisted molecular-beam epitaxy of (0001) GaN *J. Appl. Phys.* **91** 9638

[16] Mayer M 1999 SIMNRA, a simulation program for the analysis of NRA, RBS and ERDA *AIP Conf. Proc.* 475, 541–4

[17] Moram M A and Vickers M E 2009 X-ray diffraction of III-nitrides *Rep. Prog. Phys.* **72** 036502

[18] Metzger T *et al* 1998 Defect structure of epitaxial GaN films determined by transmission electron microscopy and triple-axis x-ray diffractometry *Philos. Mag. A* **77** 1013–25

[19] Sánchez A M, Molina S I, Pacheco F J, García R, Sánchez-Garcia M A, Sánchez F J and Calleja E 2000 Si doping effect on the defect structure in GaN/AlN/Si(111) heteroepitaxial systems *Bol. Soc. Esp. Cerám. Vidrio* **39** 468–71

[20] Feldman L C, Mayer J W and Picraux S T 1982 *Material Analysis by Ion Channeling* (New York: Academic)

[21] Contreras-Puente G *et al* 2012 Raman measurements on GaN thin films for PV-purposes *38th IEEE Photovoltaic Specialists Conference.* 000036–8

[22] Chine Z, Rebey A, Touati H, Goovaerts E, Oueslati M, Jani B E and Laugt S 2006 Stress and density of defects in Si-doped GaN *Phys. Status Solidi* **203** 1954

[23] Kisielowski C *et al* 1996 Strain-related phenomena in GaN thin films *Phys. Rev. B* **54** 17745

[24] Zhao D G, Jiang D S, Yang H, Zhu J J, Liu Z S, Zhang S M, Liang J W, Li X, Li X Y and Gong H M 2006 Role of edge dislocations in enhancing the yellow luminescence of *n*-type GaN *Appl. Phys. Lett.* **88** 241917

[25] Cremades A, Görgens L, Ambacher O, Stutzmann M and Scholz F 2000 Structural and optical properties of Si-doped GaN *Phys. Rev. B* **61** 2812

[26] Feneberg M *et al* 2014 Band gap renormalization and Burstein-Moss effect in silicon- and germanium-doped wurtzite GaN up to 10^{20} cm^{-3} *Phys. Rev. B* **90** 075203